



HAL
open science

A new approach to thermal history modelling with detrital low temperature thermochronological data

Kerry Gallagher, Mauricio Parra

► **To cite this version:**

Kerry Gallagher, Mauricio Parra. A new approach to thermal history modelling with detrital low temperature thermochronological data. *Earth and Planetary Science Letters*, 2020, 529, pp.115872. 10.1016/j.epsl.2019.115872 . insu-02317389

HAL Id: insu-02317389

<https://insu.hal.science/insu-02317389v1>

Submitted on 16 Oct 2019

HAL is a multi-disciplinary open access archive for the deposit and dissemination of scientific research documents, whether they are published or not. The documents may come from teaching and research institutions in France or abroad, or from public or private research centers.

L'archive ouverte pluridisciplinaire **HAL**, est destinée au dépôt et à la diffusion de documents scientifiques de niveau recherche, publiés ou non, émanant des établissements d'enseignement et de recherche français ou étrangers, des laboratoires publics ou privés.

Manuscript Number: EPSL-D-19-01000R1

Title: A new approach to thermal history modelling with detrital low temperature thermochronological data

Article Type: Letters

Keywords: detrital thermochronology; thermal history; inversion

Corresponding Author: Professor Kerry Gallagher,

Corresponding Author's Institution: University of Rennes 1

First Author: Kerry Gallagher

Order of Authors: Kerry Gallagher; Mauricio Parra

Abstract: We present an inverse modelling strategy to infer thermal history information from detrital low temperature thermochronological data from modern sediment sampling the outlet of a single catchment. As presented, the method relies on the assumption that the geological timescale thermal history was the same across the catchment. The detrital sample is assumed to represent a mixture of grains originating from a potentially unknown sampling of the present elevation range in the catchment. The approach also implements a method to infer a function describing the topographic sampling represented in the detrital sample. In practice, this may reflect variations in erosion with elevation but also lithological differences in the catchment (fertility) and the nature of erosion/transport processes in the catchment. A combination of detrital and in-situ bedrock data are recommended to improve the resolution of the topographic sampling function. We demonstrate the application of the approach to a set of fission track data from the Fundacion catchment in the Sierra Nevada de Santa Marta in northern Colombia. The inferred thermal history suggest a period of rapid cooling initiated around 50-30 Ma, followed by slower cooling to the present day, consistent with the regional geological history. The topographic sampling function estimates suggest that the hypsometric distribution is not appropriate in terms of the contributions from different elevations to the detrital sample. Rather, the data imply a higher proportion of sampling from lower elevations close to the location of the outlet where the detrital sample was collected.

1 **A new approach to thermal history modelling with detrital**
2 **low temperature thermochronological data**

3

4

Kerry Gallagher¹ and Mauricio Parra²

5

6

1. Géosciences Rennes/OSUR, University of Rennes, Rennes, 35042, Rennes, France

7

kerry.gallagher@univ-rennes1.fr

8

9

2. Institute of Energy and Environment, University of São Paulo, Av. Prof. Luciano Gualberto
1289, Cidade Universitária, 05508-010, Sao Paulo-SP-Brazil

10

mparra@iee.usp.br

11

12

Corresponding author : Kerry Gallagher (kerry.gallagher@univ-rennes1.fr).

13

14

15 **Abstract**

16 We present an inverse modelling strategy to infer thermal history information from detrital
17 low temperature thermochronological data from modern sediment sampling the outlet of a
18 single catchment. As presented, the method relies on the assumption that the geological
19 timescale thermal history was the same across the catchment. The detrital sample is assumed
20 to represent a mixture of grains originating from a potentially unknown sampling of the
21 present elevation range in the catchment. The approach also implements a method to infer a
22 function describing the topographic sampling represented in the detrital sample. In practice,
23 this may reflect variations in erosion with elevation but also lithological differences in the
24 catchment (fertility) and the nature of erosion/transport processes in the catchment. A
25 combination of detrital and in-situ bedrock data are recommended to improve the resolution
26 of the topographic sampling function. We demonstrate the application of the approach to a set
27 of fission track data from the Fundación catchment in the Sierra Nevada de Santa Marta in
28 northern Colombia. The inferred thermal history suggest a period of rapid cooling initiated
29 around 50-30 Ma, followed by slower cooling to the present day, consistent with the regional
30 geological history. The topographic sampling function estimates suggest that the hypsometric
31 distribution is not appropriate in terms of the contributions from different elevations to the
32 detrital sample. Rather, the data imply a higher proportion of sampling from lower elevations
33 close to the location of the outlet where the detrital sample was collected.

34

35 **Keywords : Detrital thermochronology, thermal history, inversion**

36

37

38 **1. Introduction**

39 Since the seminal papers defining the concept and calculation of closure temperature
40 (Dodson, 1973) and early applications of the concept (e.g. Wagner et al. 1977), one of the
41 main uses of temperature dependent geochronology, or thermochronology is to recover
42 information on the thermal histories of rocks. In doing this we exploit the fact that different
43 dating systems, defined by a combination of a specific mineral and isotope decay scheme, are
44 sensitive to different temperature ranges. This temperature sensitivity is generally manifested
45 in terms of losing the daughter product by some kind of thermally activated diffusion process,
46 and leads to a measured age younger than the formation age of the host rock. For high
47 temperature systems such as zircon U-Pb, the measured age is often interpreted as the time at
48 which the host rock cooled below the appropriate closure temperature. The closure
49 temperature is a function of cooling rate, grain size and dating system specific kinetic and
50 geometry parameters as defined by Dodson (1973) and for zircon U-Pb is nominally around
51 1000-1100°C (e.g. Schoene 2014).

52 Low temperature thermochronology is typically defined to include apatite and zircon
53 (U-Th)/He and $^4\text{He}/^3\text{He}$ dating, apatite and zircon fission track analysis and feldspar K-Ar and
54 $^{40}\text{Ar}/^{39}\text{Ar}$ dating (see Reiners and Ehlers, 2005). These particular systems are sensitive to
55 temperatures from near surface temperatures ($\sim 30\text{-}40^\circ\text{C}$) to a maximum around 400°C but are
56 also characterised by a large range in temperature sensitivity relative to the nominal closure
57 temperature, referred to as the partial annealing zone for fission track analysis and the partial
58 retention zone for noble gas diffusion. This range in temperature sensitivity, and so loss of
59 daughter product, is then manifested as a progressive decrease in measured age depending on
60 how long a given rock sample has resided in, or has taken to cool across, the partial
61 retention/annealing zone.

62 For surface or bedrock samples collected from different elevations in a given
63 catchment or valley, this effect is typically represented as a vertical profile in which age
64 increases with elevation (e.g. Wagner and Reimers, 1972, Fitzgerald, et al. 1995, Valla et al.
65 2010). Often there is a change inferred in the slope of the age-elevation relationship, such that
66 the lower part of the profile has a steeper slope than the upper part. This can be interpreted as
67 either a change in erosion rate, an exhumed partial retention/annealing zone or more generally
68 as a combination of both. Such interpretations can be made in a relatively qualitative sense
69 (e.g. Fitzgerald et al. 1995), or in a more quantitative sense, typically involving the inference
70 of the cooling and/or erosion history through forward or inverse thermal history modelling
71 (Ehlers 2005, Gallagher et al. 2005, Valla et al. 2010, Braun et al. 2012, Fox et al. 2014).

72 As it is generally erosion that controls the cooling history recorded in low temperature
73 thermochronometers, an obvious extension of the vertical profile approach is to consider the
74 products of erosion, i.e. detrital thermochronology. Early applications of detrital
75 thermochronology considered distributions of single grain ages from sediments for different
76 closure temperature systems such as zircon U-Pb, mica and feldspar $^{40}\text{Ar}/^{39}\text{Ar}$, or zircon and
77 apatite helium dating or fission track analysis, and relating these to possible source regions
78 over geological time (e.g., Ross and Bowring 1990, Copeland and Harrison 1990, Garver and
79 Brandon 1994, Carter and Bristow 2000, Tranel et al. 2011, Enklemann and Ehlers 2015,
80 Malusà and Fitzgerald 2019).

81 Furthermore, efforts have been made to exploit the distribution of detrital ages
82 measured in modern sediments to inform us about the nature of erosion and tectonic processes
83 in the recent geological past by predicting the expected distribution of detrital ages for a range
84 of thermochronometric systems, including some of the lower temperature systems such as
85 apatite (U-Th-Sm)/He (AHe) and apatite fission track (AFT) data. These predictions are often
86 made using local vertical age profiles (Brewer et al., 2003, Ruhl and Hodges 2005, Stock et

87 al. 2006, Huntington and Hodges 2006, Malusà and Fitzgerald 2019) or using predictions as a
88 2D age-elevation surface, the ages being predicted from landscape and/or 3D thermal models
89 (e.g. Whipp et al 2009, Ehlers et al. 2015). These approaches require some form of
90 assumptions, either *a priori* or *a posteriori*, about the nature of sampling of the age-elevation
91 distribution. This has commonly been taken to be the hypsometric distribution by default. In
92 this case, the detrital ages are assumed to be a mixture of ages from either a predicted or
93 observed age-elevation relationship, sampled according to the proportion of the present
94 topography in a given elevation range over the area of the relevant catchment or drainage
95 basin. A different approach was implemented by Avdeev et al. (2011) and Fox et al. (2015) in
96 which they inferred a distribution of age-elevation relationships and how these could be
97 sampled over different elevations, as a function of variable erosion rate, to reproduce both
98 detrital and in situ bedrock age data. More recently, Braun et al. (2018) and Gemignani et al
99 (2018) proposed a form of statistical un-mixing of downstream variations in measured detrital
100 ages which does not require any assumption about the sampling of topography. However, this
101 approach requires multiple detrital samples and the drainage system to traverse several (sub)-
102 catchments, or regions, contributing different cooling signals to the final distribution.

103 Here we propose an inverse method to infer the thermal history from a modern detrital
104 sample from a single catchment. In this case, the implicit assumption is that any thermal
105 history information recorded in the modern sediment reflects the same long term thermal
106 history experienced by bedrock samples in the catchment. The motivation for this approach is
107 firstly to assess whether modern detrital samples can provide similar thermal history
108 information as a typical bedrock vertical profile. A lack of bedrock samples occur due to the
109 inaccessibility of some source regions, e.g. under ice as highlighted by Enkelmann and Ehlers
110 (2015), or for logistical reasons (cost, access). In the absence of bedrock samples, we will
111 need to make an assumption about how erosion processes sample the present day catchment

112 topography. We will use the phrase topographic sampling function (TSF) to describe the
113 sampling of the in situ or bedrock vertical profile data to produce modern sediment detrital
114 data. To relax the assumption that we know *a priori* this topographic sampling function, the
115 method we present allows us to treat this as an unknown. As we will focus on low
116 temperature thermochronometers, specifically apatite fission track analysis and apatite (U-Th-
117 Sm)/He dating, it is important also to note a potential sampling bias related to variable
118 concentrations of a specific mineral (e.g. apatite), or fertility in the source region (e.g. Tranel
119 et al. 2011) and the effects of hydraulic sorting of different grain-size fractions (e.g. Malusà
120 and Garzanti 2019). Thus any inferred topographic sampling function will reflect a
121 combination of modern erosion and transport processes acting on the catchment and the
122 fertility of bedrock outcropping across it.

123 In the following, we describe the method we have developed to deal with extracting
124 thermal history information from detrital low temperature thermochronological data. Here we
125 focus on AFT and AHe data in particular, but the approach is readily extended to other data
126 types (e.g. ZHe) from the outlet of a given catchment. The detrital data may also be combined
127 with in situ bedrock data (the canonical vertical profile). An implicit assumption is that the
128 distribution of ages with elevation is effectively constant (or has minor and smooth
129 variations). The approach we present also allows us to infer the topographic sampling
130 function. We show that in the case where we have both detrital and vertical profile data, this
131 approach allows us to infer the topographic sampling function with more confidence, than just
132 detrital data alone. Finally, we demonstrate the application of the method to an AFT dataset
133 from northern Colombia.

134

135

136 **2. Methodology**

137 The inverse thermal history modelling problem for a 1D vertical profile with in situ bedrock
138 samples has been previously described (Gallagher et al. 2005, Gallagher 2012) so we only
139 briefly review the main assumptions here. All samples in a vertical profile are assumed to
140 have experienced the same general form of thermal history with the difference between the
141 thermal histories for the top and bottom samples defined by a temperature gradient that may
142 vary over time. It is implicit that lower elevation samples can never have been at lower
143 temperatures than higher elevation samples. Therefore, a vertical profile can not be cut by
144 faults active over the timescale relevant to the thermal history, nor can the thermal state of the
145 bedrock have been locally perturbed, for example by hot fluid circulation. For a given thermal
146 history we can make a prediction of the AHe/AFT age and track length distribution elevation
147 profiles by exploiting the appropriate diffusion/annealing models. By suitably combining the
148 predictions over the elevation range of a given catchment, we can similarly make a prediction
149 of the detrital age distribution. Thus, the detrital data can be considered as a sampling of
150 the vertical profile data in the catchment. It is important to highlight that dispersion in such
151 detrital data will reflect the combination of grains from different elevations (hence different
152 thermal histories), but factors controlling the rates of annealing (AFT) and diffusion (AHe)
153 for each grain and also different sources of measurement error. Therefore, dispersion in AFT
154 data can occur due to variations in annealing kinetics attributable to chemical composition,
155 e.g. Cl content or a proxy compositional measure such as Dpar (Green 1988, Ketcham et al.,
156 1999, 2007), as well as the statistical variability of single grain-ages inherent in the track
157 counting process (e.g. Galbraith 2005). We allow for these factors in the method we present
158 here. AHe data can show dispersion due to variation in whole grain geometries and sizes (e.g.
159 Farley, 2000), the presence of broken grains (Brown et al. 2013,), and variable diffusion
160 kinetics due to radiation damage related effects (Flowers et al. 2009; Gautheron et al. 2009,

161 Willet et al. 2017). Here, we allow for variable grain size, but not the effects of radiation
162 damage on He diffusion in apatite nor incomplete or broken apatite grains. However, the
163 general methodology we present could deal with both of these factors at the expense of
164 increased computation time.

165

166 **2.1 The forward problem**

167 The general forward problem is illustrated in figure 1 (and see also Gallagher 2012). We
168 initially specify the model (m) as a thermal history, given by a series of time-temperature
169 points and the temperature difference, or temperature gradient, between the uppermost and
170 lowermost elevations in a hypothetical vertical profile that covers the maximum range of
171 elevation in the catchment . Combined with the appropriate diffusion/annealing models, we
172 can make a prediction of the age/length-elevation profiles. As a consequence of the factors
173 leading to dispersion described above, these will be distributions, rather than point values, at a
174 given elevation. These distributions need to be propagated into the predicted final detrital
175 age/length distributions. To generalise, we will refer to the kinetic parameter and grain size
176 variables as control variables and these will be represented by κ and the range of possible
177 values defined by κ_{min} and κ_{max} . In the following, we will present the approach considering
178 just one general control variable. Then we can write the total predicted detrital distribution,
179 conditional on the thermal history model, m , as

$$180 \quad p_{detrital}(d_p) = \int_{\kappa_{min}}^{\kappa_{max}} \int_{z_{min}}^{z_{max}} d_p(z, \kappa|m) p(z) p(\kappa) dz d\kappa \quad (1)$$

181 where $d_p(z, \kappa|m)$ is the predicted distribution for elevation z and control parameter value κ ,
182 $p(\kappa)$ is the probability distribution on the control variable, and $p(z)$ is the probability of
183 sampling from elevation z , or what we refer to above as the topographic sampling function

184 (TSF). Often the TSF is assumed to be equivalent to the hypsometric distribution. We return
 185 to this later, but for the moment we state that if we specify a thermal history and the TSF in a
 186 catchment, we can predict what age/length distributions we expect to see in a detrital sample
 187 with grains from that catchment.

188 ***2.1.1 Predicting the AFT age and length distributions***

189 For a given thermal history and kinetic parameter, we predict the noise-free fission track age
 190 and length distribution at a given elevation. For the age, we use the external detector method
 191 (EDM) age equation (e.g., Hurford and Green, 1983) to calculate the spontaneous to induced
 192 track density ratio, ρ_s/ρ_i for a given thermal history. We can convert the predicted AFT age
 193 into the equivalent ρ_s/ρ_i . Following Galbraith (2005) and Gallagher (1995), we use a
 194 binomial distribution to sample values of the spontaneous to induced track counts ratio
 195 N_s/N_i . The parameter of the binomial distribution is given as

$$196 \quad \theta = \frac{\rho_s/\rho_i}{1 + \rho_s/\rho_i} \quad (2a)$$

197 and given a selected total number of track counts, $N_s + N_i$, the probability for the number of
 198 spontaneous tracks is given as

$$199 \quad p(N_s | N_s + N_i) = \frac{(N_s + N_i)!}{N_s! N_i!} \theta^{N_s} (1 - \theta)^{N_i} \quad (2b)$$

200

201 We choose a given number of ages to sample (e.g. up to 100 grain ages for a given
 202 compositional group at each elevation), randomly select $N_s + N_i$ (from a specified range, e.g.
 203 50 and 500, or based on the range of values measured in a detrital sample), then randomly
 204 sample for N_s from the binomial distribution. The result gives a value of N_s/N_i which can
 205 then be converted into an AFT age and the error using the standard EDM error equation. We

206 repeat this process for the specified number of sampled ages and the predicted distribution is
207 then calculated by summing all the individual Gaussian distributions defined with the mean
208 equal to the individual AFT age and the calculated error as the standard deviation.
209 Alternatives to assuming a Gaussian kernel for each individual age include assuming N_s/N_i
210 is distributed as a Gaussian, or that, for a given $N_i + N_s$, N_s is binomially distributed (Brandon
211 1996, Galbraith 2005). The process of adding kernel distributions gives a continuous
212 predicted AFT age distribution for a given apatite kinetic parameter at a given elevation
213 accounting for the Poissonian variation of single-grain ages expected due to the counting
214 process. The AFT track length distributions are similarly predicted directly from the forward
215 model (e.g. Green et al. 1989, Gallagher 1995, Ketcham et al 1999) for each kinetic parameter
216 group and elevation. Next, both the age and length distributions at each elevation are then
217 combined for all control variable groups using a weighting based on the number of
218 grains/lengths in each kinetic parameter group. In practice, these groups are defined from the
219 measured values in the actual detrital sample. Finally, we combine the elevation dependent
220 distributions using the TSF as weights to produce the final detrital distribution for the AFT
221 data.

222 ***2.1.2 Predicting the AHe age distribution***

223 For a given thermal history, we predict the noise-free AHe age as a function of elevation and
224 grain size, using the spherical grain equivalent radius (Farley 2000). To predict a distribution
225 of ages for a given elevation and grain size, we resample a Gaussian distribution with a mean
226 defined by the predicted AHe age and a standard deviation of 10% of the calculated age error
227 to produce 50 single grain ages for each grain size group at each elevation. These are then
228 combined using a weighting, again based on the number of grains in each grain size group in
229 the actual detrital sample. Finally, we combine the elevation dependent distributions using the
230 TSF as weights to produce the final detrital distribution for the AHe data.

231

232 **2.2 Inverse problem**

233 The inverse problem is stated as follows: if we have a set of measured detrital AFT and AHe
234 data from a single catchment, we want to recover the catchment thermal history and also
235 potentially the topographic sampling function. We define the observed detrital data as $\mathbf{d} =$
236 $(d_1, d_2, \dots, d_i, \dots, d_N)$, a vector of length N , made up of a N_c AFT single grain ages, N_l track length
237 data and N_{He} AHe single grain ages, each with some form of explicit or implicit measure of
238 uncertainty (e.g. a reported measurement error on an AHe age, an assumed measurement error
239 on a track length, or a Poisson related distribution associated with track counts). We use the
240 forward model approach described above to predict the age/length distributions as a function
241 of elevation over the maximum elevation range of the catchment. The approach we present
242 can also incorporate any available bedrock vertical profile data in the catchment generally
243 allowing better inference of both the thermal history and the topographic sampling function.

244 ***2.2.1 Inference of the thermal history***

245 For the moment, we concentrate just of the thermal history inference problem. We implement
246 the same form of transdimensional Bayesian Markov chain Monte Carlo (MCMC) algorithm
247 described in Gallagher (2012) and we will not repeat the details. In brief, the thermal history
248 parameters are defined as an unknown number of time temperature points, each point with an
249 associated temperature gradient which may be specified to be constant or variable over time.
250 The prior distributions for these thermal history parameters are defined to be uniform, i.e.
251 equal probability between an upper and lower limit.

252 Given a thermal history model, and using d_p as a prediction (age or length) for that model, we
 253 define total predicted detrital age or length distribution for a given elevation and control
 254 variable, κ_j , as $p(d_p|\kappa_j, z)$. This can be integrated over elevation with the TSF ($= p(z)$) as

$$255 \quad p_{detrital}(d_p|\kappa_j) = \int_{z_{min}}^{z_{max}} p(d_p|\kappa_j, z)p(z)dz \quad (3)$$

256 To reduce the computational time, we can calculate the distributions for a finite number of
 257 control variable groups at a finite number of elevations. Then we can write the equation above
 258 in discrete form as

$$259 \quad p_{detrital}(d_p|\kappa_j) = \sum_{k=1}^{N_z} p(d_p|\kappa_j, z_k)p(z_k) \quad (4)$$

260 where N_z is the number of elevation groups, which is selected to cover the range of
 261 topography in the catchment of interest and we assume $p(z_k)$ is constant for each elevation
 262 group, defined by the range $z_{(k-1)/2} > z_k > z_{(k+1)/2}$ and $z_{(k-1)/2}$ is the midpoint between
 263 z_{k-1} and z_k and a similar definition for $z_{(k+1)/2}$.

264 Following on from this, we can write the total predicted detrital age or length distribution,
 265 summed over the control variables (with probability distribution $p(\kappa_j)$) as

$$266 \quad p_{detrital}(d_p) = \sum_{j=1}^{N_\kappa} p(d_p|\kappa_j)p(\kappa_j) \quad (5)$$

267 where N_κ is the number of control variable (e.g. compositional or grain size) groups, which
 268 can be based on the range of values in a given detrital sample, and $p(\kappa_j)$ is a distribution
 269 based on the number of samples with a value in a range defined by $\kappa_{j,min} < \kappa_j < \kappa_{j,max}$. We
 270 can either assign an observed datum to a given control variable group (which we do for AFT
 271 age and length data using a kinetic parameter, e.g., Cl, Dpar), or using the upper and lower
 272 limits for the group bounding a given control variable value, we can interpolate the

273 predictions for the specific value for a given grain (which we do for AHe age data for grain
274 size).

275

276 **2.2.2 Estimating the Topographic Sampling Function (TSF)**

277 We can exchange the order of the summation in equation (4) and write

$$278 \quad p_{detrital}(d_p|z_i) = \sum_{j=1}^{N_k} p(d_p|\kappa_j, z_k)p(\kappa_j) \quad (6)$$

279 and

$$280 \quad p_{detrital}(d_p) = \sum_{k=1}^{N_z} p(d_p|z_k)p(z_k) \quad (7)$$

281 From this we see there is a linear relationship between the predicted detrital distribution,
282 integrated over the range of control variables, and the topographic sampling function ($p(z)$
283 above). This lets use a linear inverse method to estimate the latter. The only complication is
284 that $p(z) \geq 0$, so we implement the iterative non-negative least squares method presented by
285 Kim et al. (2013). This gives an optimal TSF in the least squares sense in that it minimises the
286 sum of squares between the predicted and observed detrital distributions. Another approach to
287 infer the TSF is to implement a probabilistic MCMC sampling method as used by Avdeev et
288 al. (2011) and Fox et al. (2015) to constrain erosion rate over elevation with detrital
289 thermochronology, or more generally in change point modelling by Gallagher et al (2011).
290 This approach can directly represent the TSF as a weighting function over a given elevation
291 range, and using transdimensional sampling, it is possible to assess the required complexity of
292 the TSF. At this stage, we have not fully implemented this approach, as it proves to be
293 considerably more computationally intensive than the optimal least squares approach
294 mentioned above.

295 The elevations where we calculate the age or length distributions do need not correspond to
296 the elevations used to define the topographic sampling function (e.g. this could be the
297 hypsometric distribution defined at regular elevation intervals). As the predicted distributions
298 for a given control variable and elevation are smooth, we can interpolate the predicted
299 discrete ages or distributions to the intermediate elevations. We do this interpolation using the
300 approach described in Read (1999), which relies on weighted linear interpolation between the
301 cumulative distributions.

302 ***2.2.3 The likelihood function***

303 In general terms, the likelihood is a measure of how well predictions from a given model
304 represent the observed data. This can be defined (up to a constant of proportionality) as the
305 probability of having the observed data, given the predictions from a given (thermal history
306 and topographic sampling function) model. For the detrital data, we use the predicted detrital
307 age and length distributions to form the likelihood function. In the following, the distributions
308 are all normalised so they integrate to one, and can be treated as probability distributions.

309 If we consider detrital AFT data first, the i -th observation, d_i , from the j -th control variable
310 group j , κ_j , will be either a fission track single grain age or an individual track length
311 measurement and the control variable group will be defined as a range of some kinetic
312 parameter such as Cl content or D_{par} . In practice, we use the mean of the kinetic parameter in
313 the appropriate range to make the predictions for that kinetic parameter group as described
314 earlier, and this distribution is used for all observed data relevant to that group. For AHe age
315 data, we use the same interpolation procedure mentioned above such that, for a given
316 measured radius, we interpolate between the 2 distributions predicted for the two radii that
317 bracket the measured radius. The interpolated distribution, appropriate for the actual effective
318 grain radius, is used as the likelihood function for that grain. To incorporate additional control

319 variables, such as radiation damage controlled diffusion, typically parameterised by models
 320 based on effective uranium (eU) (e.g. Flowers et al; 2009, Gautheron et al. 2009), we would
 321 follow a similar approach defining a range of eU values based on those in the detrital sample.
 322 The likelihood for a given AHe age could then be based on 2D interpolation of the predicted
 323 ages as a function of grain size and eU.

324 The likelihood for a single datum, d_i , given the thermal history model, $p(d_i|m)$, can be
 325 defined as the integral or sum of the predicted distributions over elevation, for the appropriate
 326 control variable value, weighted by the topographic sampling function, $p(z_k)$, for elevation
 327 z_k

$$328 \quad p(d_i|m) = \sum_{k=1}^{N_z} p(d_i|\kappa_j, z_k, m)p(z_k) \quad (8)$$

329

330 Here we have dropped the dependence on κ_j on the left hand side as it is implicit for the given
 331 observation.

332 The definitions of the likelihood functions implicitly allow for the possibility that the
 333 probability of an observed value, with its associated control variable, may be zero over a
 334 range of elevations, i.e. the predicted distributions over that elevation range do not include the
 335 value of that observation.

336 The total likelihood is the product of all the individual likelihoods for each individual
 337 observation, given as

$$338 \quad p(d|m) = \prod_{i=1}^N p(d_i|m) \quad (10a)$$

339 In practice, the preference is to use the log likelihood, defined as

340

$$341 \quad L(d|m) = \sum_{i=1}^N \text{Ln}(p(d_i|m)) \quad (10b)$$

342

343 The methodology described here has been implemented in the software QTQt, and so the
344 inversion approach for the thermal history, implementing trans-dimensional Markov chain
345 Monte Carlo, closely follows given in Gallagher (2012). This implementation readily allows
346 detrital data and the classical in situ (bedrock) vertical profile data to be combined, as we just
347 need to add the individual sample log likelihood values for a given thermal history.

348

349 **3. Application to real data**

350 To demonstrate the application of the methodology described above, we give results using
351 synthetic AHe and AFT data in the supplementary material, showing the approach works.
352 Here we focus on a data set from the Fundación catchment in the Sierra Nevada de Santa
353 Marta in northwest Colombia (see figure 2a). This catchment an ideal location for testing our
354 method, given its small size ($\sim 14,500 \text{ km}^2$), high relief ($\sim 4 \text{ km}$), a relatively homogeneous
355 lithology with abundance of apatite-rich granitoids and gneisses and a combination of in situ
356 and detrital AFT data. The present day elevation in the catchment ranges from 180 to 3900 m
357 and in figure 2b, we show the present day hypsometry, as a cumulative distribution, which
358 shows that less than 20% of the topography is above 2500 m. Villagomez et al. (2011)
359 reported AFT data from 9 samples forming a vertical profile over an elevation range from 300
360 to 2700 m (Table S1, supplementary material). For logistical reasons, it was not possible to
361 collect samples from the last 1200 m. We have also recently produced a new suite of detrital
362 99 AFT single grain ages and 21 track length (and angle to c-axis) measurements from a

363 sample collected at the outlet of the catchment (Parra et al., in press, Tables S2, S3,
364 supplementary material). This combined data set lets us compare the thermal histories
365 inferred from the vertical profile data alone, the detrital data alone and the two data sets
366 together, as well as the case when we treat the topographic sampling function (TSF) as
367 unknown. We implement the approach described above by using hypothetical or dummy
368 samples located at 300 m intervals over the total elevation range of the Fundación catchment.
369 For a given thermal history, we predict the age and length distributions for these dummy
370 samples at each elevation, and then combine the distributions, weighted by the topographic
371 sampling function, to produce the final predicted detrital age and length distributions.
372 Initially, we fix the TSF to be equivalent to the present day hypsometry and consider only
373 inference of the thermal history. Subsequently, we relax this assumption and allow inference
374 of both the thermal history and TSF.

375 *In situ bedrock data alone*

376 In figure 3a, we show firstly the inferred expected thermal history based on the in situ vertical
377 profile AFT data of Villagomez et al. (2011). The MCMC sampler was run for 100,000
378 iterations, and the results presented here are derived from the last (post-burn-in) 50,000
379 iterations. We used the multi-compositional annealing model of Ketcham et al. (2007) with
380 D_{par} as the kinetic parameter, with values sampled from a normal distribution with the
381 measured values for the mean and standard deviation as the parameters of the distribution.
382 The inferred thermal history implies a period of rapid cooling between 50 and 30 Ma,
383 followed by a decrease in cooling rate for the uppermost samples. Using the dummy samples
384 at 300 m intervals, with a range of kinetic parameter equivalent to that measured in the
385 detrital sample, we also can predict the range of ages we expect for the dummy samples for all
386 thermal histories accepted by the MCMC sampling and these are also shown on figure 3b. The
387 thermal histories, inferred from the in situ data alone, predict a range of AFT ages whose

388 width increases with elevation above the last in situ sample at 2700 m profile. In figure 3c, we
389 show the predicted detrital age distribution for the thermal history in 3a (assuming that the
390 catchment is sampled according to the hypsometric curve). In terms of visual comparison, the
391 predicted distribution is best compared to the continuous distribution (in light blue in figure
392 3c) rather than the histogram. The continuous distribution is a kernel density representation of
393 the observed grain ages and errors, tending to smooth out isolated peaks present in the
394 histogram, which we do not expect the predicted distribution (also a kernel density
395 representation) to reproduce. The predicted distribution in this case has a peak about 20 Ma
396 older than the observed peak, and also lacks the tail of older ages ($> 60-70$ Ma). These
397 discrepancies could be due to the thermal histories not predicting old enough ages at higher
398 elevation, and/or the topographic sampling function not sampling the predicted vertical profile
399 distributions to capture the older ages at higher elevations.

400 *Detrital data alone*

401 Next we use only the catchment outlet detrital AFT data to infer the thermal history. The main
402 model run parameters were the same as the previous run and we used the hypsometric curve
403 as the TSF to produce the predicted detrital distribution. The results are shown in figure 4.
404 The thermal history also shows a cooling episode starting around 50 Ma, but does not imply a
405 change in cooling rate. As we would expect, the detrital age distribution is better reproduced
406 as just the detrital data were used for the inference of the thermal history. Using this thermal
407 history to predict the in situ vertical profile, the data from lower elevations are less well
408 predicted than the previous example while the data from the upper samples are better
409 reproduced. We can see from figure 4b that the predicted ages above 3000m are generally
410 older, and the range narrower than in the previous case. Consequently, we can reproduce the
411 older ages in the detrital sample, albeit with a relatively small proportion of the total predicted
412 elevation profile being sampled by the hypsometric curve as the TSF.

413 *In situ and detrital data jointly*

414 In this case, we combine the data from the previous two examples in a joint inversion, and
415 again using the hypsometric curve as the TSF. The results are given in figure 5. Relative to
416 the two previous examples, the inferred thermal history is most similar to the detrital data
417 only case, but with the cooling event starting a little earlier, but still around 50 Ma, and a
418 lower implied temperature gradient at that time. Relative to the detrital data only case (fig. 4),
419 the combined data reproduces the detrital age distribution less well (over-predicting the peak
420 age by about 10 Ma) and the vertical profile data better, except perhaps the uppermost in situ
421 sample. The opposite tendencies are the case relative to the in situ only results (fig. 3). Given
422 the previous results, this is not unexpected as some kind of compromise solution between the
423 two solutions based on just the in situ vertical profile or detrital data sets.

424 *In situ and detrital data jointly, and inference of TSF*

425 The results of the previous examples are based on assuming the TSF is given by the
426 hypsometric curve. Now we relax that condition and use the combined in situ and detrital data
427 to infer the TSF. To achieve this we first consider a proposed thermal history, and predict the
428 detrital distributions using the hypsometric curve as an initial TSF model. Then we use the
429 iterative non-negative least squares algorithm of Kim et al. (2013) to estimate a TSF that
430 provide the optimal fit (in the least squares sense) to the observed data. Given this least
431 squares estimate for the TSF, we calculate the likelihood for the detrital data as defined
432 earlier. The combined thermal history-TSF proposed model may or may not be accepted
433 during the MCMC sampling, as at any given iteration the acceptance or rejection of a
434 proposed model is effectively based on the likelihood function value relative to that of the
435 current model (the accepted model from the previous iteration). We present an uncertainty
436 range for the least squares TSF estimates that represents the 95% credible interval for all

437 accepted models. This implied uncertainty can be considered optimistic (too small) as we use
438 only the optimal (non-negative least squares) solutions for each accepted thermal history,
439 rather than a population of estimates that would be obtained with an MCMC sampling method,
440 as mentioned earlier.

441 The results are shown in figure 6. Now, the expected thermal history is most similar
442 to that obtained using just the in situ vertical profile data, but the peak of younger ages in the
443 observed detrital data is better reproduced. Relative to the input hypsometric curve, the
444 inferred topographic sampling function implies a greater contribution from lower elevations,
445 such that 50% comes from < 700m and correspondingly less at the highest elevation. The few
446 older detrital ages are not well predicted for the expected model, but we see the average of all
447 predicted detrital distributions does have a small contribution around 80-90 Ma.

448 The surface geology shows two main lithological groups, Precambrian gneisses with
449 amphibolite and granulite facies that occupy 22% of the total area and crop out at lower
450 elevations, and Jurassic and Triassic granitoids that constitute the rest of the catchment, at
451 both lower and higher elevations (Figure 2). Both groups contain apatite, as shown by the
452 bedrock data set used in this paper, which include samples from both lithological groups. If
453 we rule out uneven fertility the inferred TSF then implies that it is the contribution from lower
454 elevations that lets us reproduce the young peak in the detrital data. While this makes sense in
455 terms of proximity to the outlet where the detrital sample was collected, and perhaps reflects
456 local river incision, a test of this inference would be to obtain U-Pb ages on the apatite grains,
457 which would clearly distinguish the relative contributions of a Precambrian source from a
458 Triassic-Jurassic source. Furthermore, the fertility in terms of apatite yield vary significantly
459 in the same lithology (e.g. by x100, Tranel et al 2011), and a more detailed assessment of this
460 factor in the source region and its modification during transport would be required to

461 substantiate this interpretation of the inferred TSF. Finally, we assume that the TSF is the
462 same for the same elevations across the catchment.

463 The geological interpretations of the thermal history models are beyond the scope of
464 this contribution, but the inferred timing of cooling initiation from the detrital data alone is
465 consistent with that from the in situ data, but lacks the same detail on later changes in cooling
466 rate. Widespread Oligocene-Miocene (30-15 Ma) ZHe and AFT ages over a 2 km interval of
467 elevation and the lack of younger ages in the northwest Santa Marta range have been used to
468 infer this two-phase cooling, with deceleration taking place sometime in the last 15 My
469 (Villagómez et al., 2011, Patiño et al., 2019).

470

471 **4. Concluding statements**

472 We have presented a method to infer thermal histories from detrital thermochronological data
473 from a single catchment. We can model a hypothetical vertical profile, allowing for variations
474 in control variables, such as annealing kinetics for AFT, and grain size for AHe, and then
475 sample this according to a specified or inferred topographic sampling function (TSF). The
476 detrital data can also be combined with in situ bedrock thermochronological data and this will
477 yield more reliable inference of the TSF. In this contribution we use a least squares method to
478 infer an optimal TSF for a given thermal history. At the expense of greater computational
479 time, the TSF could also be sampled using a transdimensional MCMC approach such as that
480 applied to change point models (e.g. Gallagher et al. 2011, Fox et al. 2015). This would allow
481 us to estimate credible intervals on the TSF for individual thermal histories.

482 In practice an inferred TSF will potentially reflect a combination of different factors,
483 such as how erosion processes and production and transport of detrital material may vary with

484 elevation and also lithological controls on fertility and mineral fractionation/destruction
485 during transport. Depending on the scientific question of interest, the resolution of these
486 different contributing factors will require more detailed study of lithological compositions and
487 yield, and independent constraints on recent erosion rates (e.g. ^{10}Be , Fox et al . 2015)

488 A key assumption is that the thermal history is effectively the same across the
489 catchment and it is this thermal history that is represented in a catchment outlet detrital
490 sample. This could be relaxed to allow, for example, for a major fault in catchment by having
491 different thermal histories either side of the fault. This scenario then introduces more
492 complexity to the modelling process, as we need to infer the contributions from each side
493 present in a single detrital sample. Detrital sampling in upstream tributaries on both sides of
494 fault may provide additional information to help constrain the contributions in the outlet
495 sample. Overall, we suggest the approach as presented is best suited to small, confined
496 catchments with one major outlet, such as the Fundación catchment example we present here.
497 We have considered only single grain detrital data with unknown specific source regions
498 within the watershed (e.g. collected from a sand). Using aliquots of single grains separated
499 from pebbles or clasts (e.g. Fitzgerald et al. 2019) may be a useful extension of this approach
500 as such each aliquot will necessarily come from the same source region in the catchment.
501 Recent developments in analytical methods such LA-ICP-MS methods for fission track and
502 He dating provide additional data such as apatite U-Pb ages and REE spectra for the same
503 grains used for detrital thermochronology. Such data would also provide independent
504 information on potential source regions within a catchment, particularly if combined with
505 similar data from in situ samples. Finally, the approach we have presented could, in principle,
506 be applied to older sediments. However, in the absence of bedrock thermochronometry (and
507 other independent detrital source rock data), the TSF will clearly be less well constrained. To
508 estimate the TSF, we also need to specify the effective elevation range sampled by the

509 sediments. The structure of the inferred TSF will depend on that range and is validity difficult
510 to assess in the absence of information on the proportions and fertility of different source rock
511 lithologies. Also, we would also need to allow for the post-depositional thermal history. If the
512 sediments have not been buried deep enough to sample the relevant partial annealing or
513 retention zones, then this may have a relatively minor effect in terms of recovering the pre-
514 depositional thermal history. However, increasing burial depth will progressively overprint
515 the provenance related signal, reducing the resolution of the pre-depositional thermal history
516 to perhaps just the time the grains in the sediment cooled below the effective closure
517 temperature, or entered the partial annealing or retention zones.

518

519 **Acknowledgements**

520 We would like to thank Nathan Niemi and Matthew Fox for useful reviews that helped us
521 clarify certain aspects of this paper. Also we thank Maxime Bernard, Juan Sebastián
522 Echeverri, Ana María Patiño, Philippe Steer, and Peter van der Beek for comments and
523 discussion over the last year or so. This work was facilitated through a FAPESP-CNRS
524 binational project (FAPESP Sprint 2017/ 50276-3). M.P thanks FAPESP JP Project
525 2013/03265-5 for funding the data acquisition.

526

527 **References**

- 528 Avdeev B., Niemi, N., Clark, M.K., 2011. Doing more with less: Bayesian estimation of
529 erosion models with detrital thermochronometric data *Earth. Planet. Sci. Letts.*, 305, 385-
530 395.
- 531 Brandon, M.T., 1996. Probability plots for fission-track grain-age samples, *Rad. Meas.*, 26,
532 663-676.
- 533 Braun, J., Gemignani, L., van der Beek, P., 2018. Extracting information on the spatial
534 variability in erosion rate stored in detrital cooling age distributions in river sands. *Earth*
535 *Surf. Dyn.* 6, 257–270. <https://doi.org/10.5194/esurf-6-257-2018>.
- 536 Braun, J., van der Beek, P., Valla, P., Robert, X., Herman, F. Glotzbach, C., Pedersen, V.,
537 Perry, C., Simon-Labric, T. Prigent C. 2012. Quantifying rates of landscape evolution and
538 tectonic processes by thermochronology and numerical modeling of crustal heat transport
539 using PECUBE. *Tectonophysics*, 524-525, 1-28
- 540 Brewer, I.D., Burbank, D.W., Hodges, K.V., 2003. Modelling detrital cooling-age populations:
541 insights from two Himalayan catchments, *Basin Res.* 15, 305-320.
- 542 Brown, R.W., Beucher, R., Roper, S., Persano, C., Stuart, F., Fitzgerald, P., 2013. Natural age
543 dispersion arising from the analysis of broken crystals, part I. Theoretical basis and
544 implications for the apatite (U-Th)/He thermochronometer. *Geochimica et Cosmochimica*
545 *Acta*, 122. 478-497.
- 546 Carter A, Bristow C.S., 2000. Detrital zircon geochronology: Enhancing the quality of
547 sedimentary source information through improved methodology and combined U-Pb and
548 fission-track techniques. *Basin Res.*, 12, 47-57
- 549 Copeland, P. and Harrison, T.M., 1990. Episodic rapid uplift in the Himalaya revealed by
550 $^{40}\text{Ar}/^{39}\text{Ar}$ analysis of detrital K-feldspar and muscovite, Bengal Fan. *Geology* 18, 354-
551 357.
- 552 Dodson, M. H, 1973. Closure temperature in cooling geochronological and petrological
553 systems, *Contrib. Mineral. Petrol.*, 40, 259–274.
- 554 Ehlers, T. A., Szameitat, A., Enkelmann, E., Yanites, B. J., Woodsworth, G. J., 2015.,
555 Identifying spatial variations in glacial catchment erosion with detrital thermochronology,
556 *J. Geophys. Res. Earth Surf.*, 120, 1023–1039, doi:10.1002/2014JF003432.
- 557 Ehlers, T.A., Farley, K.A., Rusmore, M.E., and Woodsworth, G.J., 2006, Apatite (U- Th)/He
558 signal of large-magnitude accelerated glacial erosion, southwest British Columbia.
559 *Geology*, v. 34, p. 765-768.
- 560 Enklemann, E. and Ehlers, T.A., 2015. Evaluation of detrital thermochronology for
561 quantification of glacial catchment denudation and sediment mixing. *Chem. Geol.*, 411
562 299–309
- 563 Farley K.A., 2000. Helium diffusion from apatite: general behavior as illustrated by Duragno
564 fluorapatite. *J Geophys Res* 105, 2903-2914
- 565 Fitzgerald, P. G., Sorkhabi, R. B., Redfield T. F., Stump E., 1995. Uplift and denudation of
566 the central Alaska Range: A case study in the use of apatite fission-track thermo-
567 chronology to determine absolute uplift parameters. *J. Geophys. Res.*, 100, 20175–20191.
- 568 Fitzgerald, P.G., Malusà, M.G. Muñoz, J.A., 2019. Detrital thermochronology using
569 conglomerates and cobbles IN : Malusà, , M.G. and Fitzgerald, P.G. (Editors), *Fission-
570 Track Thermochronology and its Application to Geology*, Springer International Publ.
571 AG, 295-314.

- 572 Flowers, R.M., Ketcham, R.A., Shuster, D.L., Farley, K.A. 2009. Apatite (U-Th)/He
573 thermochronometry using a radiation damage accumulation and annealing model.
574 *Geochimica et Cosmochimica Acta*, 73, 2347-2365.
- 575 Fox, M., Herman, F., Willett, S.D., May, D.A., 2014. A linear inversion method to infer
576 exhumation rates in space and time from thermochronological data, *Earth Surf. Dynam.*, 2,
577 47-65.
- 578 Fox, M., Leith, K., Bodin, T., Balco, G. and Shuster, D.L., 2015. Rate of fluvial incision in
579 the Central Alps constrained through joint inversion of detrital ¹⁰Be and
580 thermochronometric data. *Earth Planet. Sci. Letts.*, 411., 27-36.
- 581 Galbraith, R.F., 2005., *Statistics for Fission Track Analysis*; Chapman and Hall/CRC, 240 p.
- 582 Gallagher, K. 1995. Evolving thermal histories from fission track data, *Earth Planet. Sci.*
583 *Letts.*, 136, 421-435.
- 584 Gallagher, K., 2012. Transdimensional inverse thermal history modelling for quantitative
585 thermochronology, *J. Geophys Res.* 117, B02408, doi:10.1029/2011JB00882.
- 586 Gallagher, K., Bodin, T. Sambridge, M, Weiss, D, Kylander, M, Large, D., 2011. Inference of
587 abrupt changes in noisy geochemical records using Bayesian transdimensional
588 changepoint models, *Earth Planet. Sci. Letts.*, 311, 182-194.
- 589 Gallagher, K., Stephenson, J., Brown R., Holmes, C. Fitzgerald, P. 2005. Low temperature
590 thermochronology and modelling strategies for multiple samples 1 : vertical profiles,
591 *Earth Planet Sci. Letts.*, 237, 193-208.
- 592 Garver J.I., Brandon M.T., 1994. Fission-track ages of detrital zircon from Cretaceous strata,
593 southern British Columbia: Implications for the Baja BC hypothesis. *Tectonics* 13, 401-
594 420
- 595 Gautheron, C., Tassan-Got, L., Barbarand, J., Pagel, M. 2009. Effect of alpha-damage
596 annealing on apatite (U-Th)/He thermochronology. *Chemical Geology*, 266, 157-170.
- 597 Gemignani, L., van der Beek, P.A., Braun, J. Najman, Y., Bernet, M., Garzantie, E. and
598 Wijbrans, J.R., 2018. Downstream evolution of the thermochronologic age signal in the
599 Brahmaputra catchment (eastern Himalaya): Implications for the detrital record of
600 erosion. *Earth. Planet. Sci. Letts.*, 499, 48-61.
- 601 Gómez, J., Montes, N.E., Nivia, Á. & Diederix, H., compilers. 2015. Geological Map of
602 Colombia 2015. Scale 1:1 000 000. Servicio Geológico Colombiano, 2 sheets. Bogotá.
- 603 Green P.F., 1988. The relationship between track shortening and fission track age reduction in
604 apatite: combined influences of inherent instability, annealing anisotropy, length bias and
605 systems calibration. *Earth Planet Sci Lett* 89, 335-352
- 606 Green P.F., Duddy I.R., Laslett G.M., Hegarty K.A., Gleadow A.J.W., Lovering J.F. 1989.
607 Thermal annealing of fission tracks in apatite 4. Quantitative modeling techniques and
608 extension to geological timescales. *Chem Geol* 79, 155-182
- 609 Huntington, K. W., Hodges, K.V. 2006. A comparative study of detrital mineral and bedrock
610 age-elevation methods for estimating erosion rates, *J. Geophys. Res.*, 111, F03011,
611 doi:10.1029/2005JF000454.
- 612 Hurford, A. J., and Green, P. F., (1983), The zeta age calibration of fission-track dating:
613 *Isotope Geoscience*, v. 1, no. 4, p. 285-317.
- 614 Ketcham, R.A., Carter, A., Donelick, R.A., Barbarand, J., Hurford, A.J., 2007. Improved
615 modeling of fission-track annealing in apatite. *American Mineralogist* 92, 799–810.

- 616 Ketcham, R.A., Donelick, R.A., Carlson, W.D., (1999). Variability of apatite fission-track
617 annealing kinetics. III. Extrapolation to geological timescales. *American Mineralogist* 84,
618 1235–1255.
- 619 Kim, D., Sra, S., Dhillon, I.S., 2013., A non-monotonic method for large-scale non-negative
620 least squares. *Optimization Meth. & Software*, 28, 1012-1039.
- 621 Malusà, M.G. and Garzanti, E. 2019. The Sedimentology of Detrital Thermochronology, IN :
622 Fission-Track Thermochronology and its Application to Geology, Malusà, M.G. and
623 Fitzgerald, P. (Editors) 123-143
- 624 Malusà, M.G. and Fitzgerald, P.G. 2019. Application of Thermochronology to Geologic
625 Problems : Bedrock and Detrital Approaches, IN : Malusà, M.G. and Fitzgerald, P.G.
626 (Editors), Fission-Track Thermochronology and its Application to Geology, Springer
627 International Publ. AG, 191-200.
- 628 Parra, M., Echeverri, S., Patiño, A.M., Ramírez-Arias, J.C., Mora, A., Sobel, E.R., Almendral,
629 A., Pardo, A., in press, Cenozoic Evolution of the Sierra Nevada de Santa Marta, In:
630 Gómez Tapias, J., Almanza, M.F., Ochoa, A. (eds), The Geology of Colombia Book,
631 Servicio Geológico Colombiano.
- 632 Patiño, A. M., Parra, M., Ramírez, J. C., Sobel, E. R., Glodny, J., Almendral, A., and
633 Echeverri, S., (2019), Thermochronological constraints on Cenozoic exhumation along
634 the southern Caribbean: The Santa Marta range, northern Colombia, in Horton, B. K., and
635 Folguera, A., eds., *Andean Tectonics*, Elsevier, p. 103-132. Read, A.L. 1999. Linear
636 interpolation of histograms, *Nucl. Instr. and Methods in Physics Res. A* 425, 357-360.
- 637 Reiners, P.W., Ehlers, T.A., 2005. Low-Temperature thermochronology : Techniques,
638 Interpretations, and Applications. *Reviews in Mineralogy and Geochemistry*, v. 58, 1.
639 Min. Soc. Am. Geochem Soc.
- 640 Ross, G.H.M., Bowring, S.A., 1990. Detrital Zircon Geochronology of the Windermere
641 Supergroup and the Tectonic Assembly of the Southern Canadian Cordillera, *J. Geology*,
642 98, 879-893.
- 643 Ruhl, K.W., Hodges, K.V., 2005. The use of detrital mineral cooling ages to evaluate steady
644 state assumptions in active orogens: An example from the central Nepalese Himalaya.
645 *Tectonics* 24, 1-14.
- 646 Schoene, B. (2014) U–Th–Pb Geochronology, *Treatise on Geochemistry*, Volume 4 : the
647 Crust, Ch. 4.10, 341-378.
- 648 Stock, G.M., Ehlers, T.A., Farley, K.A., 2006. Where does sediment come from? Quan-
649 tifying catchment erosion with detrital apatite (U–Th)/He thermochronometry. *Geology*
650 34, 725–728.
- 651 Tranel, L.M. Spotila, J.A., Kowalewski, M.J., Waller, C.M. 2011. Spatial variation of erosion
652 in a small glaciated basin in the Teton Range, Wyoming, based on detrital apatite (U-
653 Th)/He thermochronology. *Basin Research*, 23, 571-590.
- 654 Valla, P.G., Herman, F., van der Beek, P.A., Braun, J., 2010. Inversion of
655 thermochronological age-elevation profile to extract independent estimates of denudation
656 and relief history I: Theory and conceptual model, *Earth Planet. Sci. Letts.*, 295, 511-522
- 657 Villagomez, D., Spikings, R., Mora, A., Guzman, G., Ojeda, G., Cortés, E., van der Lelij, R.
658 2011. Vertical tectonics at a continental crust- oceanic plateau plate boundary zone:
659 Fission track thermochronology of the Sierra Nevada de Santa Marta, Colombia,
660 *Tectonics*, 30, TC4004, doi:10.1029/2010TC002835

661 Wagner G.A., Reimer G.M., 1972. Fission track tectonics: The tectonic interpretation of
662 fission track apatite ages, *Earth Planet. Sci. Letts.* 14(2), 263-268.

663 Wagner G.A., Reimer G.M., Jager E., 1977. Cooling ages derived by apatite fission track,
664 mica Rb-Sr, and K-Ar dating: the uplift and cooling history of the central Alps. *Mem.*
665 *Inst. Geol. Mineral. Univ. Padova* 30:1-27

666 Whipp, D. M., Jr., Ehlers, T.A., Braun, J., Spath, C. D. 2009. Effects of exhumation
667 kinematics and topographic evolution on detrital thermochronometer data, *J. Geophys.*
668 *Res.*, 114, F04021, doi:10.1029/2008JF001195.

669 Willett, C.D., Fox, M., Shuster, D.L., 2017. A helium-based model for the effects of radiation
670 damage annealing on helium diffusion kinetics in apatite. *Earth. Planet. Sci. Letts.*, 477,
671 195-204.

672

673

674 **Figure Captions**

675 Figure 1.

676 The conceptual model to predict detrital distributions for thermochronological data.

677 (a) Yellow stars represent a typical in situ or bedrock vertical profile, that may not cover the
678 whole elevation range in a catchment. The green star represents a modern sediment detrital
679 sample from the outlet of the catchment. To model the detrital sample, we use a set of
680 hypothetical of dummy samples spanning the total elevation range of the catchment.

681 Given a specified thermal history (b), and the hypothetical samples, we can predict an age
682 elevation profile (c) for AFT and AHe (and similarly for track length distributions, not
683 shown), using a range of control variables (CV). These are kinetic parameters for AFT and
684 grain size for AHe. In practice the control variables are defined from the values and groups
685 defined for a real detrital sample. This allows us to produce a set of AHe and AFT ages for
686 the dummy samples at each elevation. Note that these predictions do not contain any
687 statistical dispersion.

688 (d) By resampling the predicted ages for each control group variable at each elevation 50-100
689 times and adding expected statistical variations, we can produce a distribution of ages for
690 each control group variable. These are then summed, weighted by the specified proportion of
691 each CV group (the thick line in (d)).

692 (e) We produce CV weighted distributions for each elevation

693 (f) These are summed over the elevation range and weighted by the topographic sampling
694 function (TSF) to give a prediction of the detrital distribution for AHe and AFT at the outlet
695 of the catchment.

696

697 Figure 2.

698 (a) Location of in situ (blue circles) and detrital (yellow circle) samples, with the AFT
699 central ages, recalculated from the data of Villagomez et al. (2011), in the Fundación
700 catchment (black outline) and a geological map (modified from Gómez et al. 2015) for the
701 Santa Marta de Sierra Nevada, northern Colombia. SMB = Santa Marta Boundary fault.

702 (b) Present day distribution of elevation (SRTM 90m), or hypsometry, in the Fundación
703 catchment. The black line is a running mean, and the red line is the cumulative distribution of
704 elevation.

705 Figure 3.

706 (a) Inferred thermal history from just in situ bed rock samples from the Fundación catchment.
707 The blue and red lines indicate the thermal histories for the uppermost and lowermost
708 elevation bedrock samples, with the 95% credible range on each. The grey lines are for other
709 in situ samples in the vertical profile, while the yellow lines are thermal histories for dummy
710 samples. The red box is the prior distribution for time-temperature points, and the black box is
711 an initial constraint to force the thermal history to start at a temperature the total
712 annealing/degassing temperatures for fission tracks and He in apatite.

713 (b) Observations and predictions using the thermal history in (a). Blue circles = observed AFT
714 ages, red diamonds = observed AFT Mean track length (MTL). The predictions are shown by
715 the dashed lines. The predicted AFT ages also include those for the dummy samples and the
716 horizontal lines show the 95% credible range on the predicted age at each elevation for all
717 accepted thermal histories.

718 (c) Predicted detrital AFT age distribution using the thermal history in (a), assuming the
719 topographic sampling function (TSF) is the present day hypsometry (see figure 2). The
720 histogram and light blue line represent the observed detrital AFT ages. The red line is the
721 predicted distribution for the thermal history in (a), and the black line is the average of the
722 predicted detrital distributions for all accepted thermal histories.

723

724 Figure 4

725 (a) Inferred thermal history from just the detrital sample at the outlet of the Fundación
726 catchment. See the caption for figure 3 for more details.

727 (b) Observations and predictions using the thermal history in (a).

728 (c) Predicted detrital AFT age distribution using the thermal history in (a), assuming the
729 topographic sampling function (TSF) is the present day hypsometry.

730

731 Figure 5

732 (a) Inferred thermal history from both the in situ samples and the detrital sample at the outlet
733 of the Fundación catchment. See the caption for figure 3 for more details.

734 (b) Observations and predictions using the thermal history in (a).

735 (c) Predicted detrital AFT age distribution using the thermal history in (a), assuming the
736 topographic sampling function (TSF) is the present day hypsometry.

737

738 Figure 6

739 (a) Inferred thermal history from both the in situ samples and the detrital sample at the outlet
740 of the Fundación catchment, allowing for the TSF to be different to the present day
741 hypsometry. See the caption for figure 3 for more details.

742 (b) Observations and predictions using the thermal history in (a) and the inferred TSF shown
743 in (c).

744 (c) Predicted detrital AFT age distribution using the thermal history in (a), together with the
745 inferred TSF, estimated with a non-negative least squares method, using the present day
746 hypsometry as a starting model. See main text for details.

747

Figure 1
[Click here to download Figure: Figure 1.pdf](#)

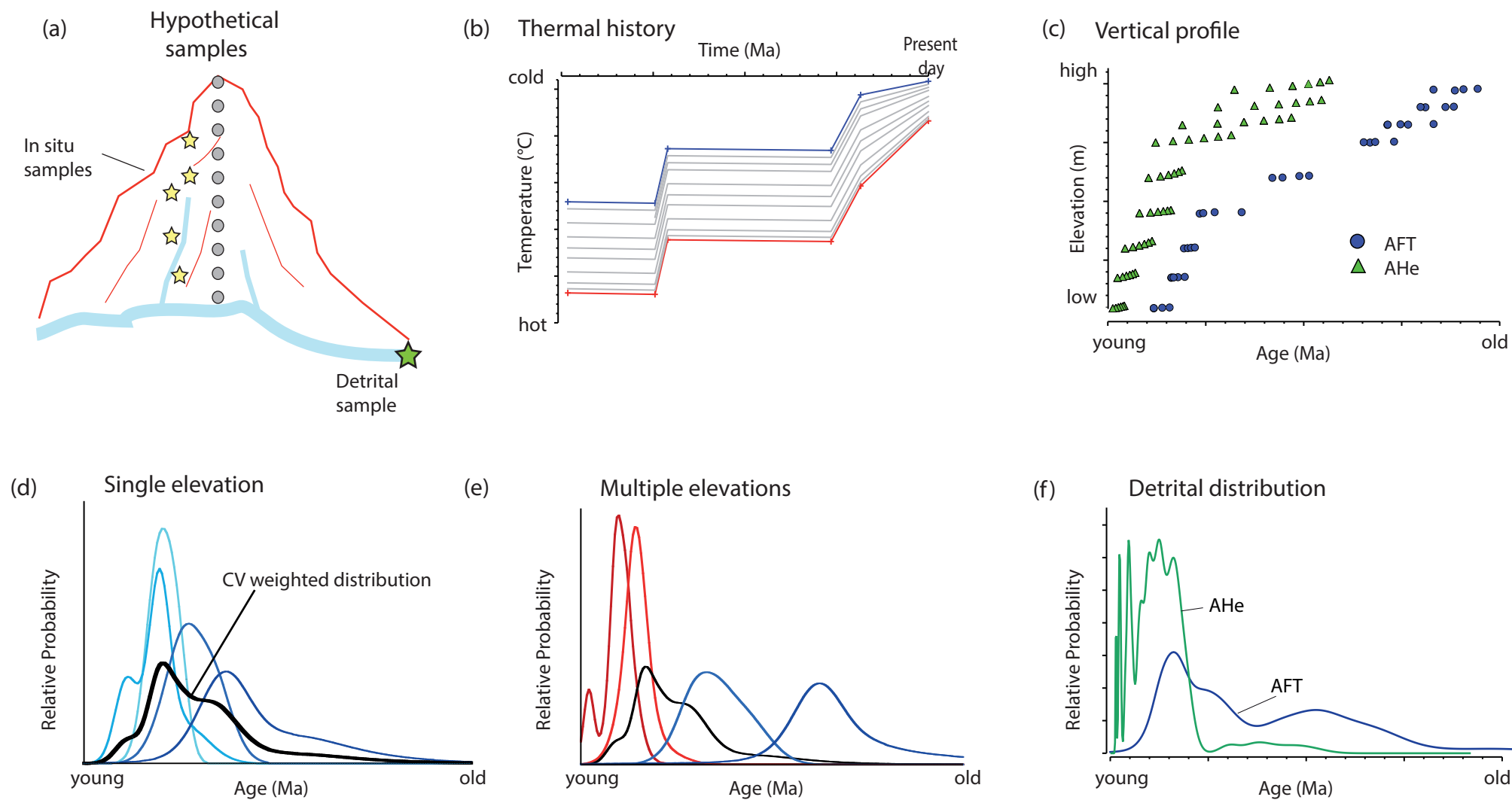


Figure 1

Figure 2
[Click here to download high resolution image](#)

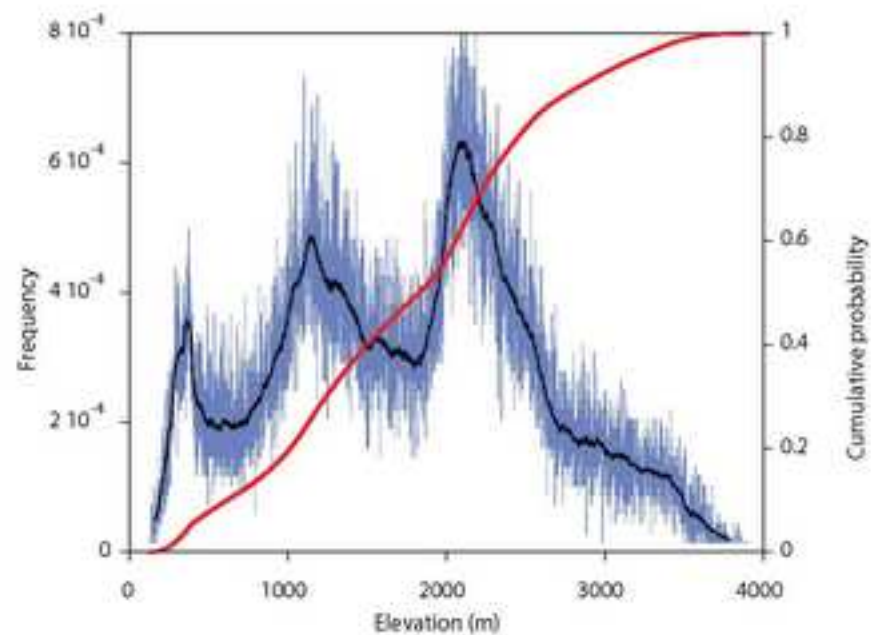
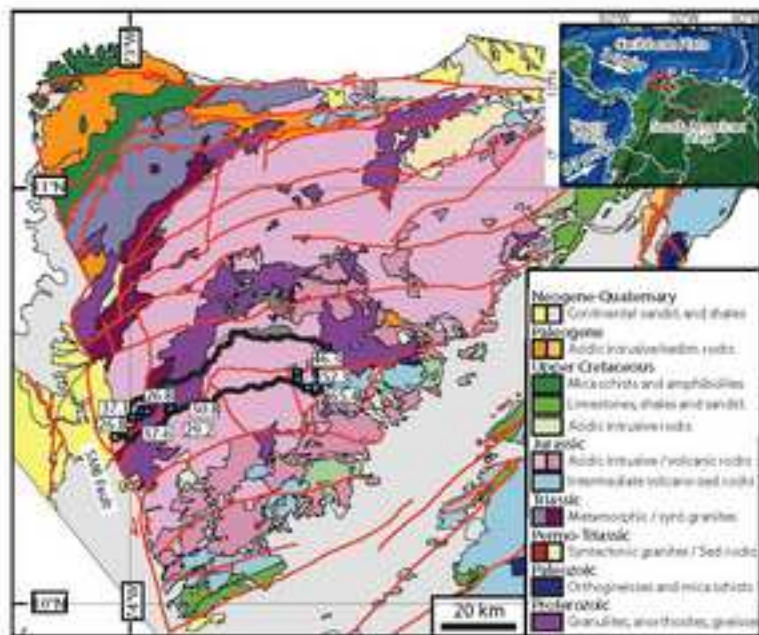


Figure 2

Figure 3
[Click here to download Figure: Figure 3.pdf](#)

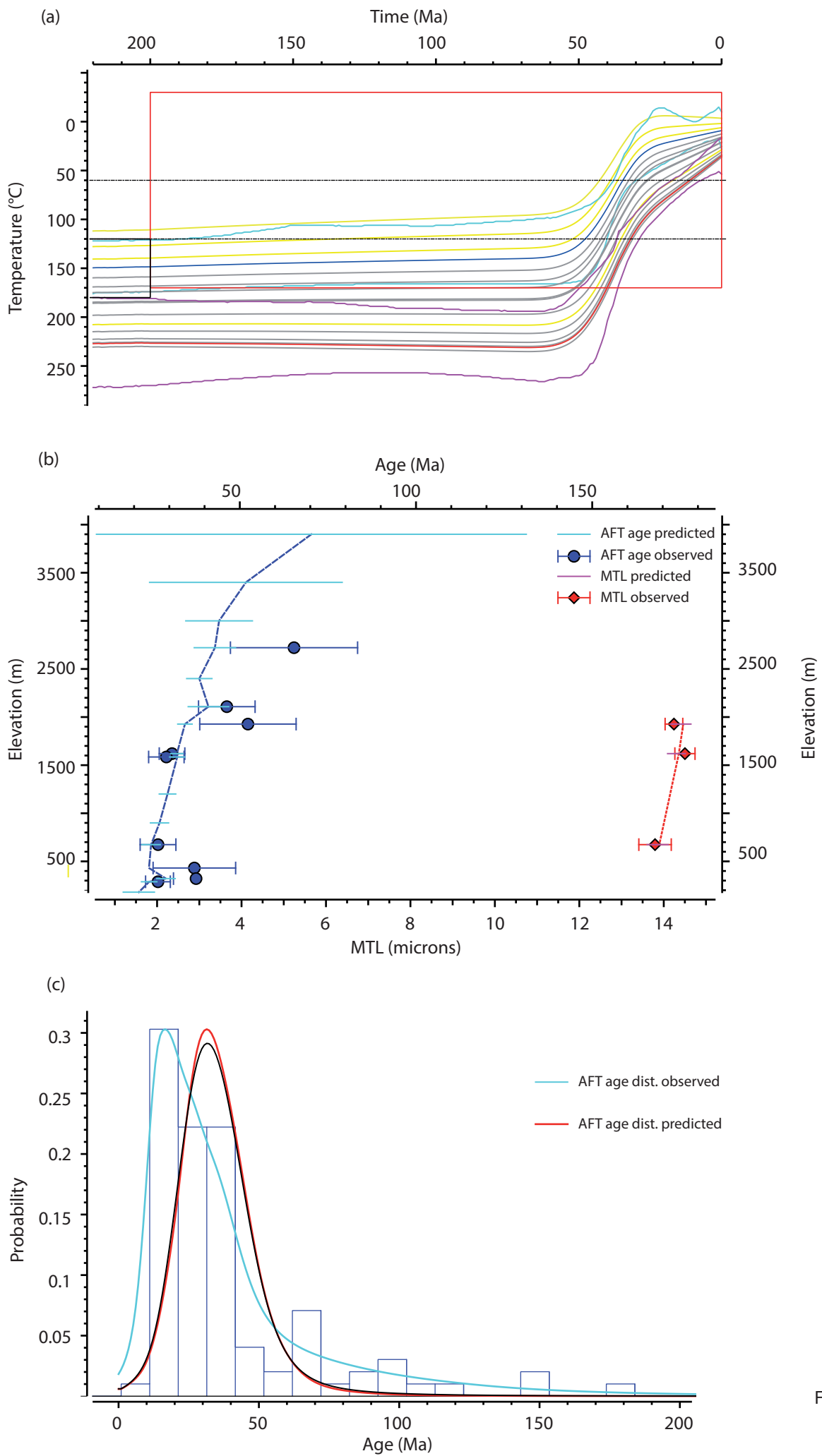


Figure 3

Figure 4
[Click here to download Figure: Figure 4.pdf](#)

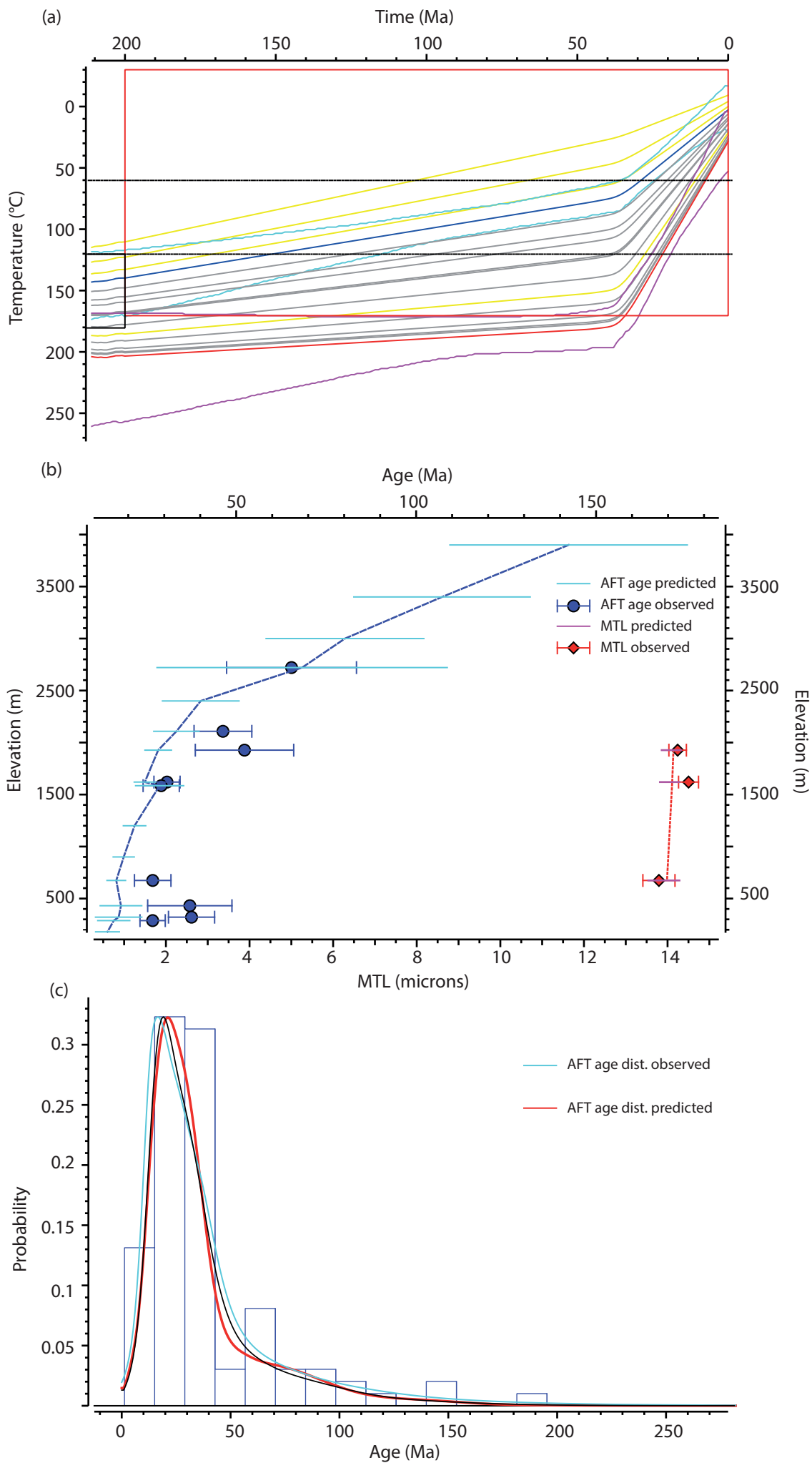


Figure 4

Figure 5
Click here to download Figure: Figure 5.pdf

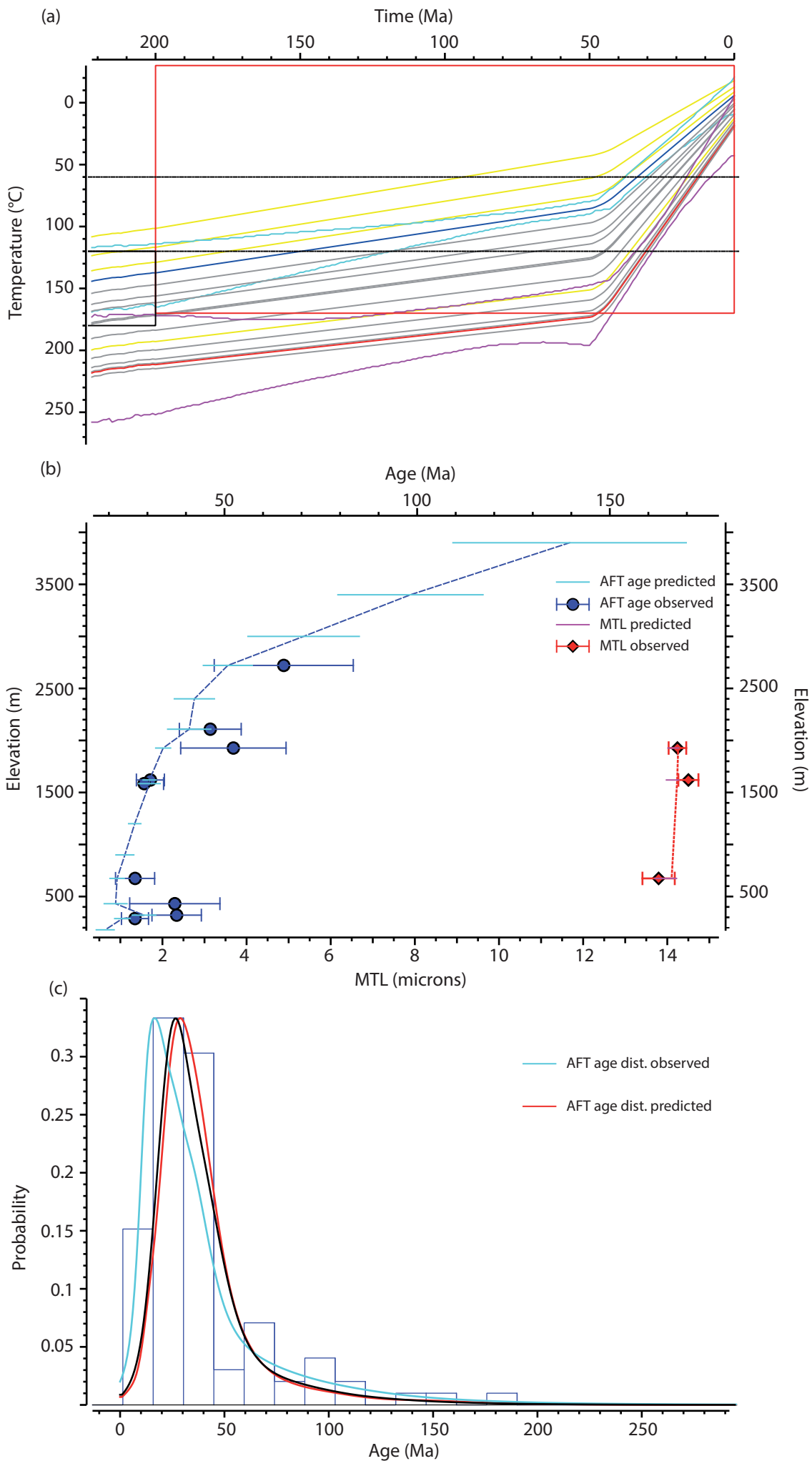


Figure 5

Figure 6
[Click here to download Figure: Figure 6.pdf](#)

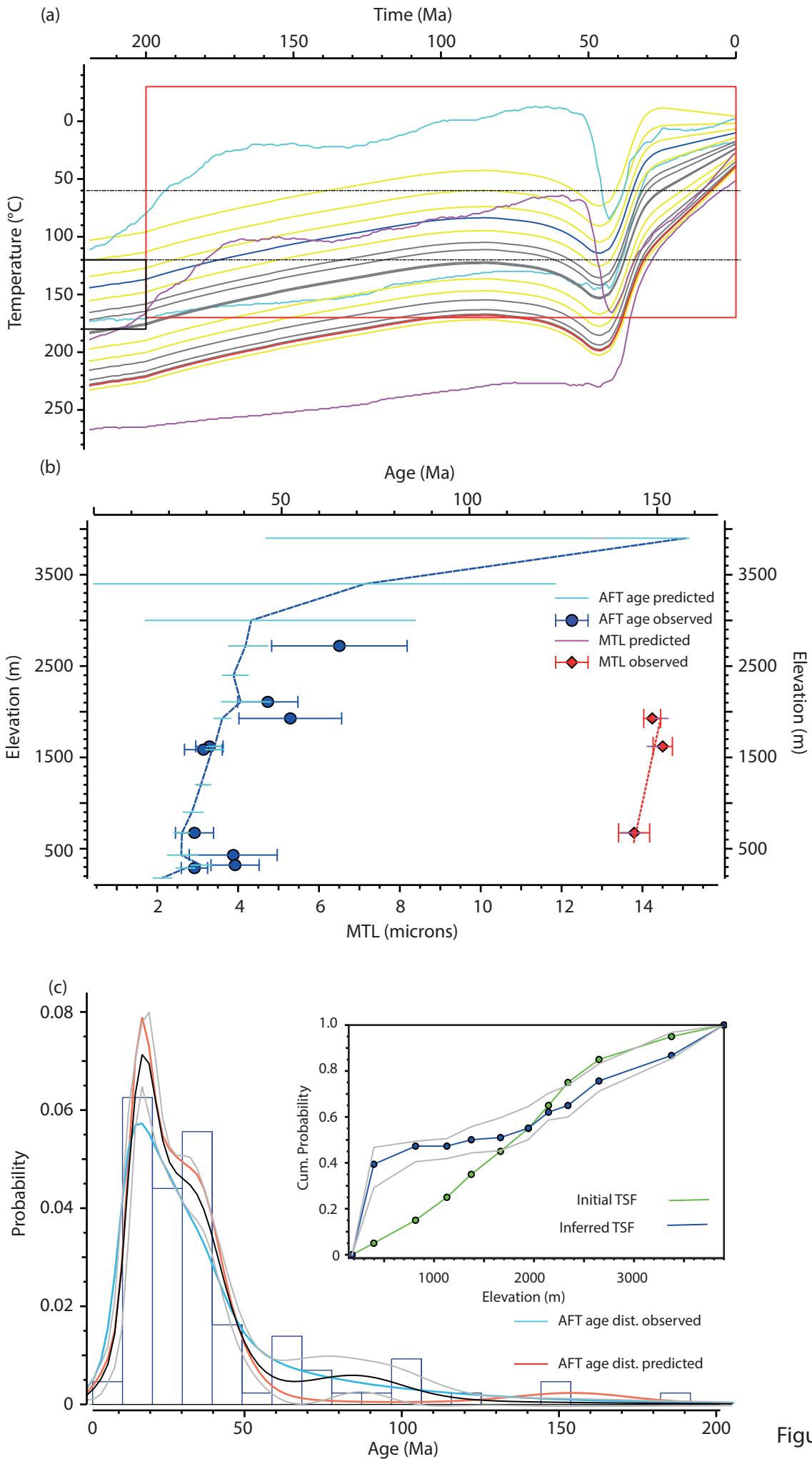


Figure 6

Figure 2 (high-resolution)

[Click here to download Figure \(high-resolution\): Figure 2_\(high res\).pdf](#)

Supplementary material for online publication only

[Click here to download Supplementary material for online publication only: Gallagher_Parra_Supplementary Material.docx](#)